



**HOPKINS STUDENT  
WIND ENERGY TEAM**

## **Technical Design Report**

Johns Hopkins University (JHU)  
Collegiate Wind Competition 2023

Submitted May 4th, 2023

Report prepared by:  
Justin Lee, Aerodynamics Lead  
Isaac Lee & Eleni Daskopoulou, Electronics and Controls Leads  
Evan LaTourrette-Ghez & David Corrente, Generator Leads  
Kathy Cao, Structures Lead

With guidance from Dr. Dennice Gayme and Dr. Rui Ni, Faculty Advisors



## Table of Contents:

<b>1 Executive Summary</b>	<b>2</b>
<b>2 Technical Design</b>	<b>2</b>
<b>2.1 Design Objective</b>	<b>2</b>
<b>2.2 Rotor and blades</b>	<b>2</b>
2.2.1 Aerodynamic Design and Analysis	2
2.2.2 Testing Methods and Results	3
2.2.3 Nose Cone Design and Testing	3
2.2.4 Rotor and Assembly	4
<b>2.3 Generator and Powertrain system</b>	<b>5</b>
2.3.1 Generator Modeling	5
2.3.2 Generator Experimental Testing	5
2.3.3 Converting and Stabilizing Power	7
<b>2.4 Electronics and Controls</b>	<b>7</b>
2.4.1 Turbine Electronics	7
2.4.2 Load Electronics	8
2.4.3 Safety System	9
2.4.4 Firmware	10
<b>2.5 Structures</b>	<b>11</b>
2.5.1 Offshore Foundation Design, Fabrication, and Testing	11
2.5.2 Yaw System Design	13
2.5.3 Tower-Base Assembly	13
<b>2.6 Enumeration of Influence of Previous Design Reports</b>	<b>13</b>
<b>2.7 Static Performance Analysis</b>	<b>14</b>
2.7.1 Cp-TSR curve	14
2.7.2 Annual Energy Production	15
<b>3 Full Turbine Integration</b>	<b>15</b>
<b>3.1 Integration</b>	<b>15</b>
<b>3.2 Distributed team management</b>	<b>16</b>
<b>4 Commissioning Checklist</b>	<b>16</b>
<b>5 Turbine Testing Results</b>	<b>17</b>
<b>5.1 Power Curve Testing</b>	<b>17</b>
<b>5.2 Durability</b>	<b>18</b>
<b>6 Appendix</b>	<b>18</b>
<b>6.1 Appendix A: Expected mechanical loads and safety factors</b>	<b>18</b>
<b>6.2 Appendix B: Chord/twist optimization and blade geometry from QBlade</b>	<b>20</b>
<b>6.3 Appendix C: FEA of TSR4 blades under centrifugal load (2740 RPM)</b>	<b>20</b>
<b>6.4 Appendix D: UMD Wind Tunnel Test Setup and Measured Deflection using a DSLR camera with a telescoping lens</b>	<b>20</b>
<b>7 References</b>	<b>1</b>

# 1 Executive Summary

For our entry to the Collegiate Wind Competition, the JHU team aimed to maximize the efficiency of an off-shore wind turbine that complies with the space and structural requirements of the competition's rules and requirements.

Our turbine blades are modeled from the S1210 airfoil at the tip and the Wortmann FX63-137 airfoil at the root, which have been tested for low-Reynolds number applications for small-scale wind turbines. This hybrid blade design was aimed to provide structural integrity for the mounting geometry towards the root region. The final blade design was 3D printed with PC Blend, chosen after multiple failure tests with different filament materials.

We use a store-bought brushless DC motor as our generator that was selected after extensive modeling and wind tunnel testing. Its three-phase power output is then rectified and smoothed to approximate a DC output. We used theoretical modeling of various motors, then tested best performers to ultimately choose the BL23E48.

Our turbine is operated by two microcontrollers: one in the turbine and one outside the wind tunnel. These microcontrollers control the blade pitch and load resistance (respectively) based on the measured wind speed, in order to optimize power output. For the safety task, braking is accomplished by feathering the blades and engaging a fail-safe caliper disc brake.

For the offshore fixed bottom foundation component we designed a suction caisson-type foundation. We also designed a more streamlined nacelle to decrease the overall drag force on the foundation and accommodate the new design choices.

## 2 Technical Design

### 2.1 Design Objective

For the 2023 Collegiate Wind Competition, our goals are to build a turbine that can produce optimal power for our system in the power production task and to pass the rated power, safety, durability, and foundation success tasks without losing any points. For power production and control, we have a custom hybrid blade design with a structural airfoil at the base and a high-performance airfoil at the tip, an active control system that maximizes power through blade pitching and varying generator load resistance, and a pitot tube to measure wind speed. For the safety task, we are using a dual braking system that implements blade feathering and a fail-safe mechanical brake. Finally, for the durability and foundation success task, we are using a suction caisson-type foundation with tested survivability and blade feathering and a streamlined nacelle to minimize drag on the turbine.

### 2.2 Rotor and blades

#### 2.2.1 Aerodynamic Design and Analysis

In this year's competition, our goal was to enhance our blade design and build upon the successes of previous years, ensuring greater structural integrity without compromising aerodynamic performance. Although the NACA 6409 from last year performed well, it proved to be too thin and fragile after repeated use. We began the new blade design process by researching airfoils used in low Reynolds number applications and for small-scale wind turbines, and chose SG6403 [1], Wortmann FX63-137 [2], and S1210 [3] airfoils. To maximize the structural integrity of our blades, we decided to use the FX63-137 airfoil for the root region for its higher relative profile thickness.

We used QBlade to model the blade geometries with the Reynolds number set to around 37,000, based on the average chord length of last year's blades as well as an average velocity of 10 m/s. The blade

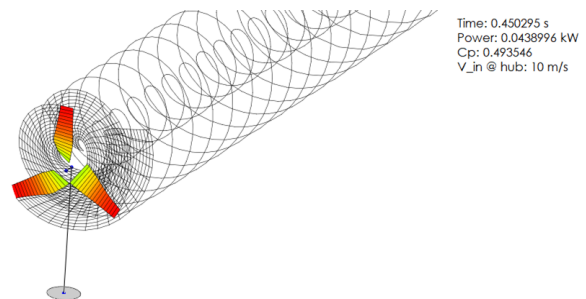


Figure 1. LLT simulation for S1210 airfoil

length was set to 18 cm to ensure that our rotor fit within the 45cm diameter tolerance, taking into consideration our pitch hub radius of around 3.5 cm. The initial tip and root chord lengths were set to around 3.5 cm and 7 cm, respectively, which approximately matches the dimensions of the blades we've been using in previous years. Initially, we set the input TSR parameter to 3, based on generator tests from the previous year. We then used QBlade's Schmitz optimization process function to generate the optimal twist and chord length at each of the 17 discretized segments along the blade length (Appendix B).

We further conducted computational analyses using QBlade's lifting-line-theory (LLT) function (Figure 1) to simulate and compare the theoretical performances and power production of the SG6403 and S1210 airfoils. We determined the S1210 airfoil was most suitable for the turbine because of its promising power coefficients. Therefore, we decided to use a hybrid blade design with the FX3-137 airfoil for the root and the S1210 for the tip. The profiles are shown below in Figure 2.

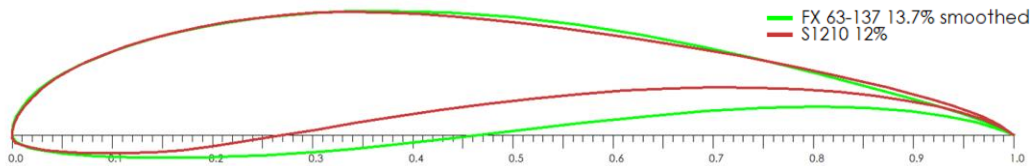


Figure 2. S1210 and FX63-137 airfoil profile

The initial blade design was optimized for a TSR of 3 on QBlade, based on generator testing from the previous year. After iterative testing in our wind tunnel (which yielded TSR values ranging from 3 to 4), we decided to model and test different blade geometries optimized for a higher TSR. However, TSR 3.4 and 4 blades could not cut in at 5 m/s. Therefore, after testing three potential blade geometries (Figure 3), we confirmed that a TSR of 3 was optimal for our turbine and wind speed conditions

### 2.2.2 Testing Methods and Results

We conducted a series of tests in JHU's wind tunnel to evaluate the power performance of our turbine blades and rotor system at varying wind speeds, mainly from 5 - 11 m/s. A linear actuator was used to pitch the blades while the load, voltage, current and rotor RPM were recorded for analysis. We further monitored the blades' performance under all of our wind tunnel tests operating at varying wind speeds (totaling >10 hours) and found no sign of cracks or yielding.



Figure 3. Blade geometries by TSR

### 2.2.3 Nose Cone Design and Testing

Inspired by a project done by GE [4], we decided to test a nose cone (dome) that would attach to the front of the rotor hub. The goal was to minimize any losses in the rotor swept area and potentially redirect more wind flow to the tip region of the blade, where most of the power is produced. We modeled and 3D-printed the nose cone to fit over the rotor head diameter (Figure 4), then installed a male threaded heat insert that screws into the rotor head.

After testing the turbine in the tunnel at 5 and 11 m/s, we compared the effect of the nose cone and determined a consistent 5% to 7% improvement in power production, which was significant enough to implement this attachment in the new assembly.



Figure 4. GE's ecoROTR nose cone (left) and 3D-printed nose cone (right)

#### 2.2.4 Rotor and Assembly

The JCZK 300RC helicopter rotor hub [5] was used to achieve active pitch control, which is the same modified hub we have been using in previous years. Pitching allows us to control the rotor speed at different wind speeds to control power output, as well as reduce the loads on the turbine by feathering the blades. An Actuonix L12 linear actuator attaches to a 3D-printed coupler along the rotor shaft, which activates the pitch control. Due to its consistent success and the ease of pitching mechanism we decided to keep this design.

Due to the combined loading of the wind thrust and centrifugal loads from rotation, we consistently saw failure points at the interface between the blade and the rotor hub connecting piece. This stress concentration was visualized in a finite element analysis (FEA) analysis in SolidWorks (Appendix C), where the turbine blade was set under a centrifugal load at 2740 rpm. This was an extreme case, since we do not expect our rotor to exceed 2000 rpm. The safety factor for this isolated loading condition can be seen in the table in Appendix A.

More significantly, we suspected the failure was more affected by fatigue loading under repeated wind tunnel testing. Therefore, we slightly modified the mounting geometry at the root of the blade in SolidWorks to accommodate the thicker airfoil profile and add more rigidity, shown in Figure 6. This allowed the blade to slot in tightly into the rotor hub mounting piece for a press fit in addition to the bolt to keep the blade in place.

The blades and mounting parts were 3D-printed mainly from the Prusa i3 MK3S+ printer due to its ease of use and high precision. To choose the best filament for strength, we ran destructive bending tests on blade samples printed with ABS, PC (polycarbonate) Blend, PETG, and PLA. Each blade sample was fixed horizontally at its rotor hub connection with a bench vice. To simulate the maximum thrust loads from the wind that were theoretically calculated (Appendix A), a distributed load was applied to the blades with four sets of strings until failure shown in Figure 7. As seen in Figure 7, we were confident in most filament choices but opted for ABS and PC Blend for their high safety factors. Ultimately our final blade design was printed with Prusament PC Blend for its high strength, good surface finish, and ease of manufacturing [6].



Figure 5. JCZK 300c rotor

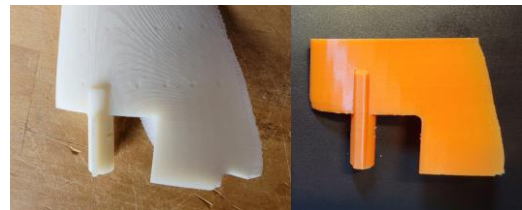


Figure 6. Mounting geometry design from prior year (left) vs. this year (right)

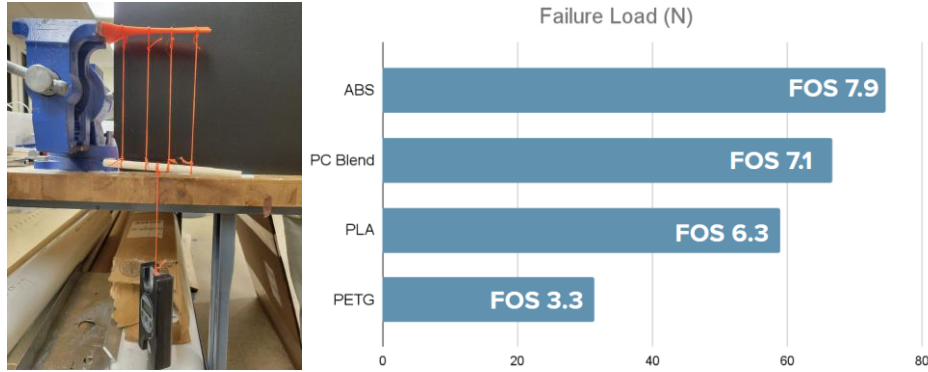


Figure 7. Blade bending test setup (left) and results (right)

## 2.3 Generator and Powertrain system

### 2.3.1 Generator Modeling

We started the year by developing a model to compare various off-the-shelf brushless DC motors prior to purchasing. To inform the model, we used last year's turbine with the newest blade design in the wind tunnel to measure the torque and rotor speed at each wind speed while optimizing blade pitch angle and load resistance for maximized power production. The previous year's generator had been tested on a dynamometer previously, so we could easily relate output current to input torque.

The model that we created uses the input torque and RPM as well as known motor characteristics such as the torque constant, back EMF constant, and the winding resistance to predict the power losses and total power generated at each wind speed. The power generated before losses was calculated using the motor constants:

$$P_{raw} = IV = \frac{k_T}{T} \cdot k_v \omega$$

where  $P_{raw}$  is the raw generated power before losses,  $I$  is the current,  $V$  is the voltage,  $k_T$  is the torque constant of the motor,  $k_v$  is the back EMF constant of the motor,  $T$  is the torque from the blades, and  $\omega$  is the rotor angular velocity. The losses due to joule heating in the generator were also calculated at each windspeed as:

$$P_{heat\ loss} = I^2 R_{winding}$$

where  $P_{heat\ loss}$  is the power lost due to joule heating in the generator, and  $R_{winding}$  is the internal winding resistance of the generator. We did not have an accurate way to predict the frictional losses in motors that we didn't yet have, so we assume a constant 12% frictional loss after research and testing last year's generator.

We could then calculate the expected power output at each wind speed from 5-11 m/s, and use the competition weighting factors to come up with a predicted score for each motor. We ran over 50 motors through this model and filtered our selections by eliminating those with an that would see a current, voltage, speed, or torque higher than the motor's rated values, as well as those that had an expected voltage higher than 48V or lower than 5V at any wind speed to comply with competition rules and ensure that our turbine electronics will be properly powered. Given these constraints, we purchased the three motors with the highest predicted power score to experimentally compare: Lin Engineering BL423E48[7], Nanotec DB87S01[8], and Nanotec DFA90S02[9].

### 2.3.2 Generator Experimental Testing

To simulate competition conditions as close as possible, we tested each motor under very similar conditions. We created a wind tunnel test stand out of T-slot framing (Figure 8) that included our whole powertrain including blades, bearings, encoder, linear actuator pitch control, and a variable load resistor. This design allowed us to 3D print different generator mounting pieces and switch out generators without changing the rest of the setup.

We set the wind tunnel to each of the competition wind speeds between 5 - 11 m/s, verifying the wind speed with a hot wire anemometer. At each wind speed, we took current and voltage measurements with multimeters and rotor speed measurements with an encoder that was calibrated with tachometer measurements. To find each generator's maximum power output, we tried every combination of blade pitch angle and load resistance for each wind speed. This allowed us to produce 3D  $C_P$  plots that show how power output varies with load and pitch angle and find the optimal combination.  $C_P$  here is defined by our generator output power over the total wind power. Figure 9 is an example of one of these plots for 11 m/s wind speed for one of the tested generators. Zero pitch angle is defined as the pitch with the optimal  $C_P$  during the variable speed region. We recorded the maximum power output at each wind speed for each of the tested generators and used the competition score weighting factors to calculate a power score to choose the generator that earned the highest power score (Table 1)—Lin Engineering BL23E48. With the chosen generator, we mapped out the optimal pitch and load resistance values for each wind speed to inform our active control system.

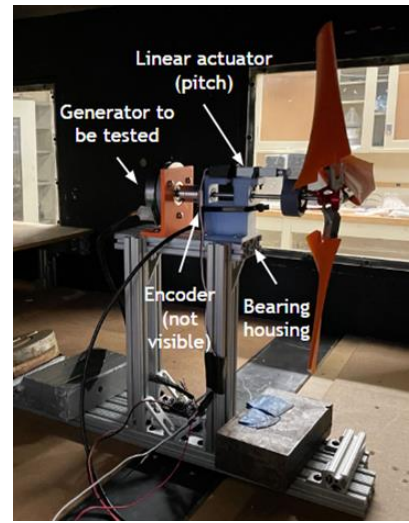


Figure 8. Wind tunnel test stand

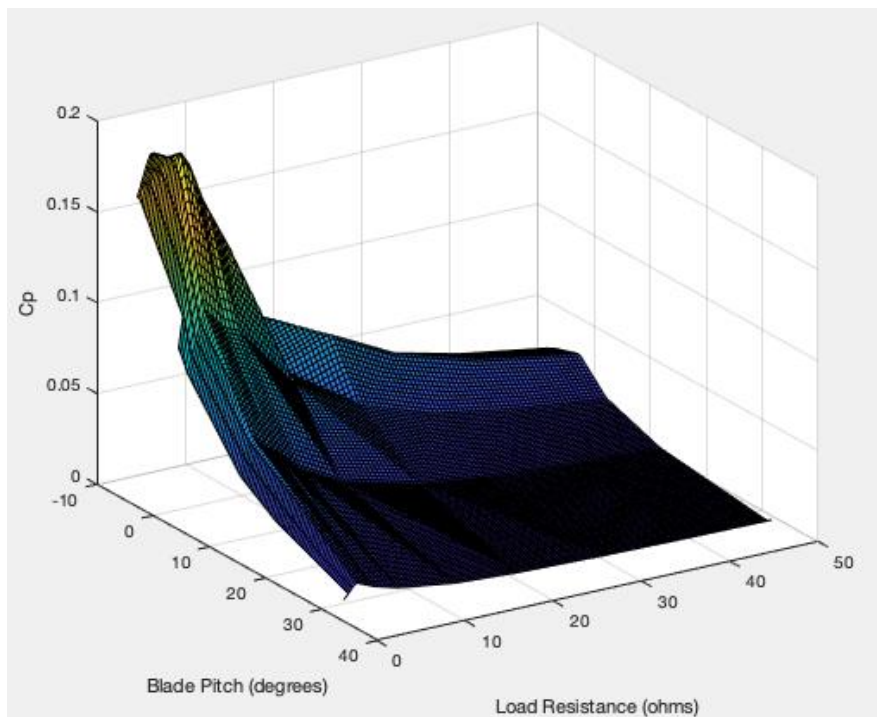


Figure 9. Example  $C_P$  vs. pitch and load resistance plot from wind tunnel test at 11 m/s

Table 1. Maximum power generated at each wind speed for each motor with estimated power score

Motor Tested	Power generated at each wind speed							Calculated Power Score
	5 m/s	6 m/s	7 m/s	8 m/s	9 m/s	10 m/s	11 m/s	
BL423E48	1.77	4.13	8.03	11.37	16.24	23.04	29.67	35.30
DB87S01	0.00	3.69	7.54	11.12	17.96	24.76	33.44	34.73
DFA90S02	0.92	3.67	5.82	8.89	13.35	21.62	24.08	28.69

### 2.3.3 Converting and Stabilizing Power

The chosen generator produces a 3-phase AC voltage which we convert to DC voltage using a 3-phase full wave rectifier. This maximizes the converted power and produces a relatively stable DC. During testing, we noticed that the periodicity of the rectified power produced by the generator compromised the stability of our power output. We thus decided to create a low pass filter by connecting a capacitor in parallel with the power line, to prevent oscillations from propagating to the PCC and our load. Competition rules allow for a  $\pm 10\%$  in power which translates to a  $\pm\sqrt{10}\%$  oscillation in voltage (which corresponds to  $V_{pp} = 0.45V$  at minimum wind speed). The oscillation frequency at minimum was calculated as  $f = \frac{\text{poles} * \text{rpm}}{120} = 22\text{Hz}$  [10]. Using the formula  $C = \frac{I}{2 * f * V_{pp}}$  (with  $I = 0.55A$  for that wind speed) we calculated the minimum required capacitance to be  $C = 0.028F$  [11]. This capacitor was added in parallel with the generator.

## 2.4 Electronics and Controls

The electronics and controls describe both the hardware and firmware developed to optimize the generated power and perform the safety task. They are divided into two critical subsystems, the turbine electronics which are located inside the nacelle, and the load electronics that simulate the power grid. Each contains an ARM M0+ processor along with peripherals to gather sensor data and control the turbine operation. This processor was selected for its low power consumption and ease of development using the Arduino IDE.

The turbine electronics are powered by the turbine generated power, while the load electronics are powered by wall power. There are 4 signal connections between the turbine and load electronics, two for the safety system and two for UART communication. All connections are optically isolated using optocouplers which utilize a photodiode and a phototransistor to convert the electrical signals to optical and then back to electrical.

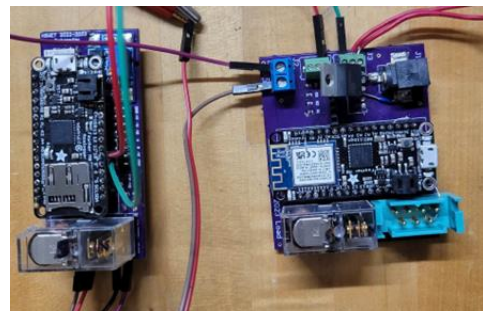


Figure 10. Turbine electronics (left) and load electronics (right)

### 2.4.1 Turbine Electronics

The main functionality of the turbine side microcontroller is the measurement of wind speed to optimize the controlled variables (pitch, load resistance) for the necessary task. Based on those measurements, the turbine detects the mode of operation (power optimization, rated power, durability) and adjusts the pitch. It also transmits the measured wind speed using the on-board hardware UART peripheral, so that the load resistance can be optimized on the load side.

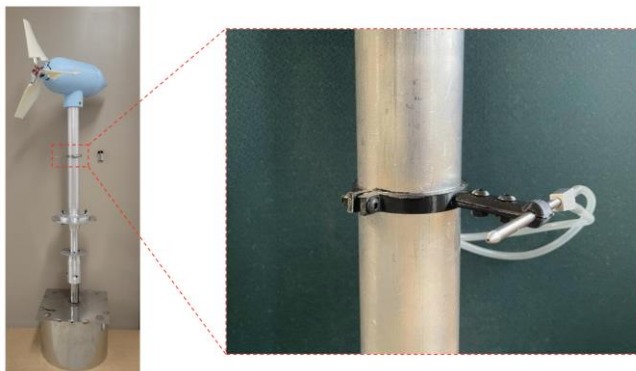


Figure 11. Pitot tube mounted on turbine tower

The primary focus when choosing a wind speed sensor was its accuracy (at least  $\pm 0.5$  m/s). Thus, we tested the performance of multiple hot-wire anemometers and pressure differential sensors. By further considering power consumption and precision of sensors, we ultimately decided to use a pitot tube with a Sensirion pressure differential sensor (with accuracy 0.13 Pa). For testing and calibration, the sensor values were compared to the values from a wall mounted hot-wire anemometer inside the wind tunnel. After ensuring accurate measurements in undisturbed air, we mounted the pitot tube to the tower of the turbine (Figure 11) and tested the effect of turbulence from

pitched, spinning blades at different mounting heights along the tower. The turbulence was insignificant at wind speeds below 11 m/s, but significant noise and deviations were observed at higher speeds due to faster blade rotation (Figure 12). Thus, for wind speeds above 11 m/s, we decided to compute the quadratic fit for two different sets of data, one without spinning blades and another one with spinning blades. During operation, we will use the generator's on board encoder to determine which of the two conversion equations should be used based on the measured shaft rotation speed.

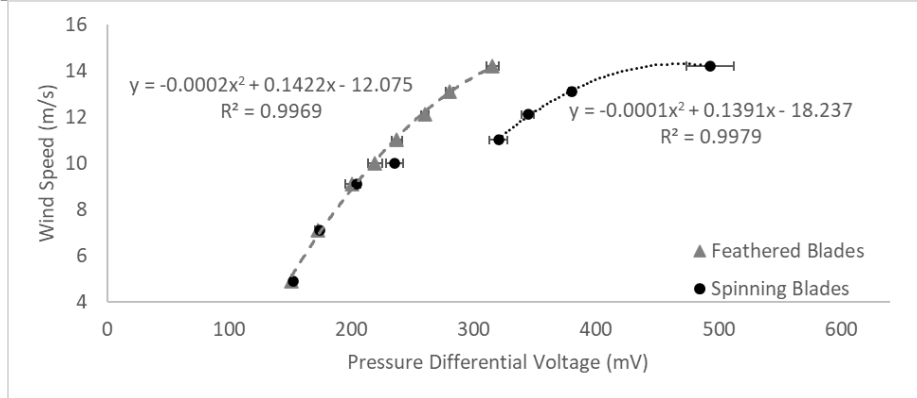


Figure 12. Wind speed vs. pitot tube pressure differential for feathered and spinning blades (using standard error)

To control the pitch, the microcontroller generates a pulse width modulated signal with the duty cycle proportionally controlling the position of the linear actuator. Extending the linear actuator pushes the rotor hub and consequently moves the blades towards the feathered position. The optimum position for each wind speed is determined by a lookup table which was generated through extensive full system testing as outlined in the generator section.

For the rated power task, the blades are actively pitched in real time, using an active feedback control loop to maintain the desired RPM from 11 m/s up to 14 m/s. The last function of the turbine electronics is monitoring the voltage generated using a voltage divider. To maintain the voltage below 48 V at all times, the electronics will pitch towards the feathered position if the generated voltage surpasses 45 V. This is a redundant protection measure since during durability testing the maximum possible generated voltage is 45.5 V. This was computed during durability testing at 22 m/s by multiplying the maximum observed shaft rotational speed (5000 RPM) with the generator's back EMF constant (9.09 V/kRPM).

#### 2.4.2 Load Electronics

During normal operation the load electronics microcontroller is receiving the UART messages from the turbine containing wind speed information. Based on the received value, the processor adjusts the load resistance value by controlling a set of 6 transistors.

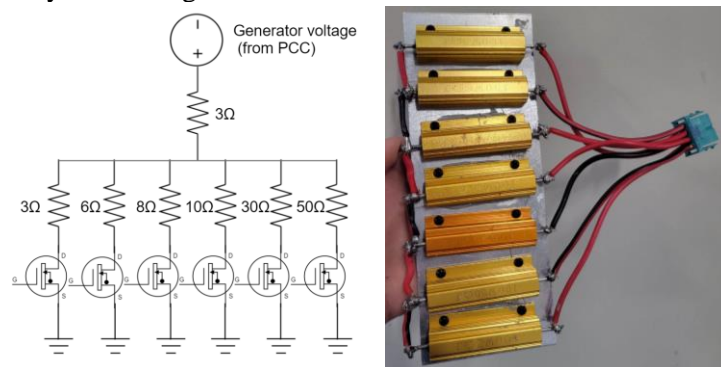


Figure 13. Schematic drawing (left) and prototype (right) of variable resistive load

To implement a high rated power variable load, we designed a custom board with seven 100W power resistors in the configuration shown in Figure 13. By controlling which transistors are connected in parallel, we can achieve resistive loads in the range of 4.3  $\Omega$  -11.3  $\Omega$  in intervals smaller than 0.5  $\Omega$ . Since most of the generated turbine power is dissipated in those resistors, we mounted them on an aluminum plate and added additional heatsinks to ensure proper heat dissipation.

### 2.4.3 Safety System

The safety system is responsible for accomplishing the brake and restart task when the safety button is pressed, or the load gets disconnected. Its components are split between the turbine and load side electronics.

The load is responsible for detecting the safety condition, by applying the turbine voltage at one side of the switch and reading the voltage on the other. The high value resistors used for the sensing voltage divider ensure that limited current passes through the safety switch. This setup detects both safety switch open circuits and load disconnects since both conditions yield a 0 V reading at the node connected to the analog input of the microcontroller. When the safety condition is detected, the load notifies the turbine microcontroller by setting the safety signal to high. When the turbine detects that rising edge, it initiates the braking process.

Our braking system primarily uses the linear actuator to feather the blades, which effectively drops the shaft rotations to an average of 7% of its original speed, below the competition’s 10% requirement. However, we also implemented a fail-safe mechanical brake in order to ensure complete braking of the turbine and to stop the turbine even in the event of total electronic system failure. We tested the full braking system and achieved complete braking of the turbine at 11 m/s within 4 seconds of safety condition initiation.

The braking mechanism uses a linear actuator to engage an RC car disc brake, which works by pulling the brake caliper’s lever to clamp onto a carbon fiber blend brake disc. The brake disc is mechanically fixed with a shaft hub onto the generator backshaft. The brake calipers and linear actuator are fixed to the nacelle with a 3D-printed PC Blend mount with 80% infill (Figure 14). To ensure alignment with the main shaft, the mount is also mechanically secured with the generator. We used an FEA (Figure 15) to further validate the mount’s structural stability for braking at maximum shaft torque (Appendix A). Additionally, conservative brake force calculations confirmed that the braking linear actuator can brake the turbine by a factor of 1.37 at the maximum torque (Appendix A).

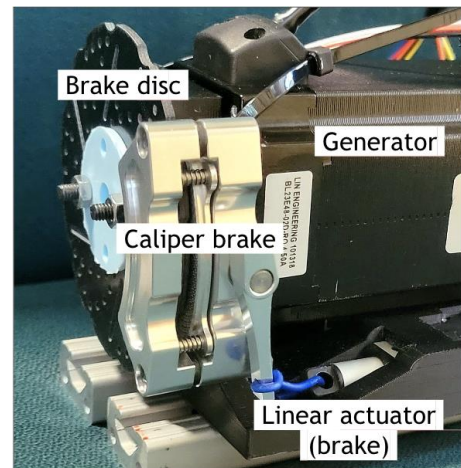


Figure 14. Full disc brake assembly with mount

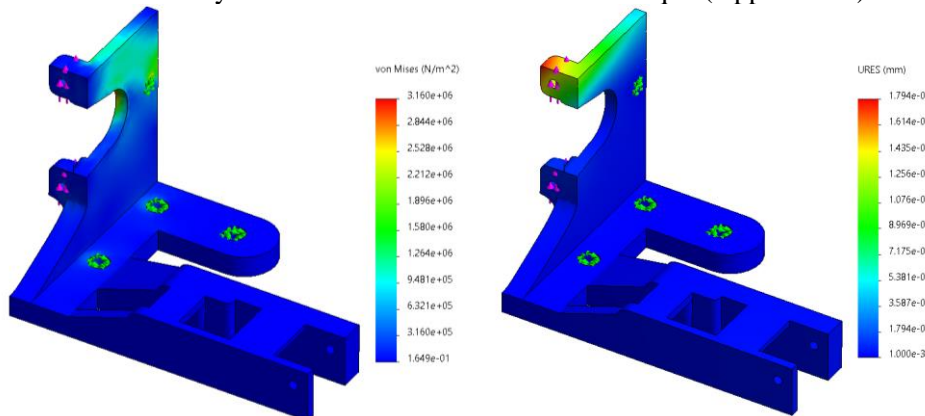


Figure 15. FEA of brake mount under maximum torque load

The circuit controlling the brake actuator is a custom design combining latching relays and two small capacitors. One capacitor is used to store the energy to be used by the linear actuator. The other is used to create a pulse for switching the latching relays. This allows us to reduce power consumption by avoiding a constant current normally required for holding relays in the make position. When the input signal becomes high, the capacitor gets connected to the actuator leads with normal polarity, causing the actuator to extend and the brake to disengage. When the input signal becomes low, or when power to the circuit is cut completely (which would be the case for complete electronics failure) the capacitor gets connected to the actuator with reverse polarity, causing the shaft to retract and the brake to engage.

The load also monitors a signal from the turbine indicating the need for external powering. During normal operation, the turbine uses the generated power. Once it brakes, that power is lost, causing the turbine electronics to turn off. When the load detects the low signal level, it flips the power relay connecting the wall power to the PCC line to power the turbine electronics (Figure 16). When the system exits the safety condition, the load notifies the turbine, which sets everything in restart condition. That includes pitching the blades to start producing power and releasing the mechanical brake. Once enough power is being produced, the load disconnects the wall power from the PCC line and the turbine connects the generator power back to the PCC line, returning to normal operation (Figure 17). All signal detection occurs using interrupts to make sure that safety related actions take priority over all other processes.

### Safety state

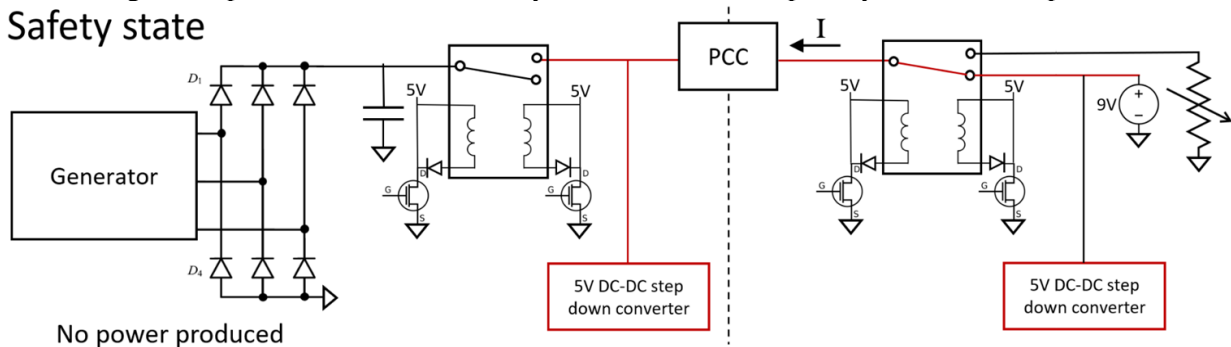


Figure 16. Powertrain diagrams for safety state operation

### Normal operation

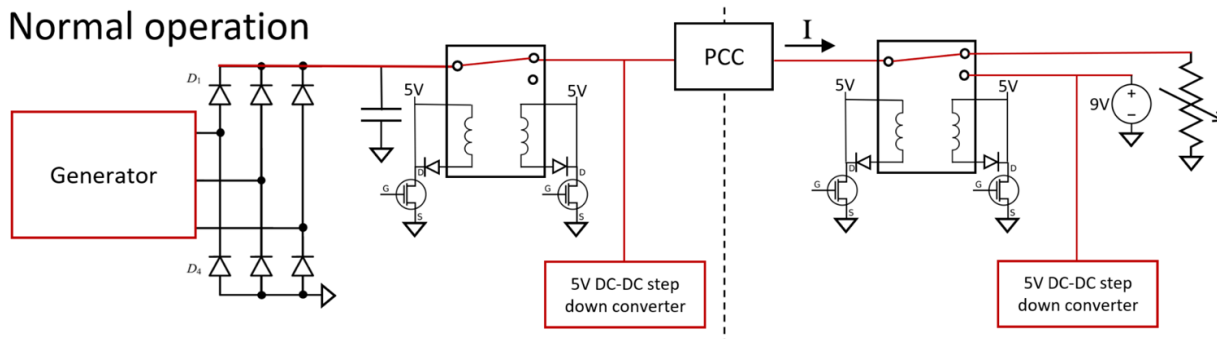


Figure 17. Powertrain diagrams for normal safety state operation

#### 2.4.4 Firmware

To perform the operations described above, both the turbine and load programs utilize a state machine to perform different actions according to the current mode of operation (normal operation, safety state, restart state) and the task that needs to be performed (optimized power, rated power, durability).

All of the above firmware was developed incrementally by testing individual systems (encoder, pressure sensor, safety system, UART etc.). After verifying the functionality of each component, we developed functions abstracting the hardware level of each task. That allowed us to easily switch out hardware components (for example the wind speed sensor), without affecting the structure of our main code. Then, we designed the state machines presented above and coded the main structure of the program,

adding the previously developed methods where necessary. Arduino libraries were used when available with the sensors and actuators selected. Finally, we tested the fully integrated system by connecting the turbine and load and verifying the ability to switch between different states and perform all the necessary tasks at bench-top and wind tunnel experiments.

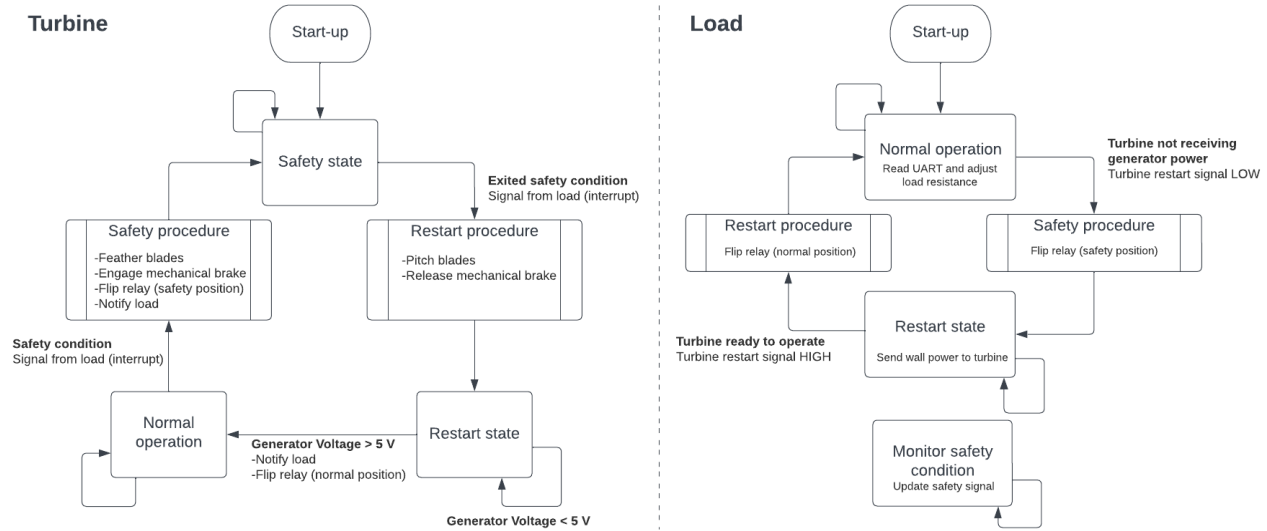


Figure 18. State machine diagram for turbine and load firmware

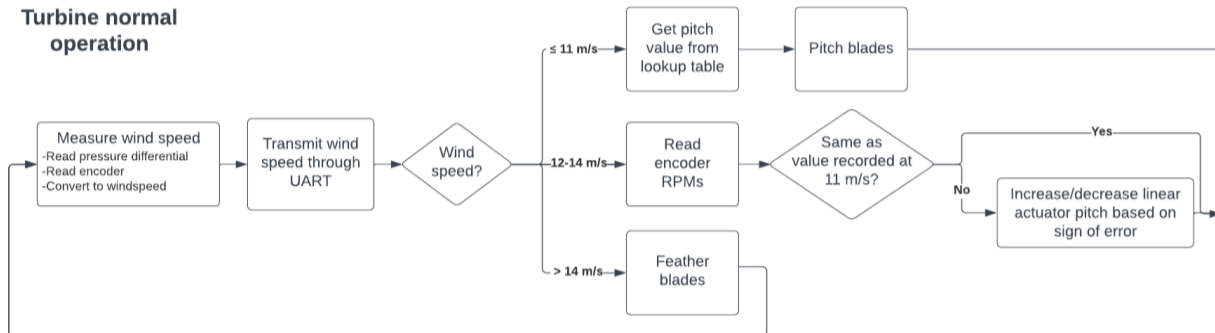


Figure 19. Block diagram of turbine for normal operation

## 2.5 Structures

The structures subsystem’s goals centered around supporting the turbine in both parked and operating conditions throughout the testing period, up to wind speeds of 22 m/s at sea level. The primary goal of the offshore foundation was to secure the turbine in the simulation tank with zero horizontal displacement. The secondary goals of the foundation were to minimize mass and facilitate installation.

### 2.5.1 Offshore Foundation Design, Fabrication, and Testing

Based on the poor performance of the team’s screw pile type foundation in last year’s competition and a thorough review of last year’s reports from all of the competitors, we conducted a more thorough analysis of the sand and pivoted to a caisson type foundation. We calculated the shear strength of the sand using the following equation [12]:

$$s = c' + (\sigma - u)\tan\phi'$$

where  $c'$  is the effective cohesion,  $\sigma$  is the total normal stress acting on the shear surface,  $u$  is the pore water pressure, and  $\phi'$  is the effective friction angle. Assuming the sand is cohesionless, in drained conditions, and of class SM, the shear strength of the sand is 870 Pa. Over the 30 cm by 30 cm allowable

foundation area, the sand would have a resistance force of 78.4 N, which is more than required based on our theoretical thrust calculations.

The caisson foundation was chosen for its relatively low weight, ease of installation, and minimal slight compaction of the sand. By pushing the foundation directly into the sandbed, we would introduce additional stress in the sand that would benefit the foundation's strength. An initial prototype was made from HVAC ductwork to validate the concept, shown in Figure 20. This prototype was made from a 12-inch pipe and cap, putting it 0.48 cm over the CWC's 30 cm width limit. However, we considered this size difference to be negligible in analyzing the performance.

We performed static loading tests in the JHU Department of Civil Engineering's Soil Lab. We used a tank similar in size to that at the CWC: the tank was 24 in long by 24 in wide by 18 in tall and filled with sand and water to depths given by competition regulations. After installation, 4 kg of weights were placed on top of the stub to simulate the weight of the turbine. Then, lateral load was applied by tying a cable to the top of the stub and hanging a bucket to be filled with sand over the side of the tank with a pulley. The foundation was loaded incrementally with sand until the foundation deflected 25 mm in the horizontal direction and deflection was measured with a digital dial gauge.



Figure 20. HVAC ductwork foundation prototype

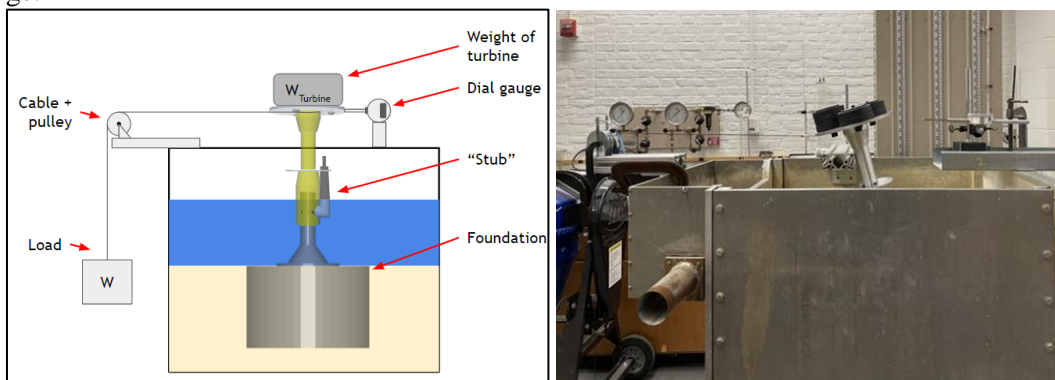


Figure 21. Diagram of test setup (left) and foundation loaded to failure (right)

Results from static testing (Figure 21) showed a conservative safety factor of 1.3 relative to the theoretical maximum thrust on the turbine at 22 m/s (Appendix A). These results informed our decision to continue with a caisson-type foundation.

Our final caisson design, shown in Figure 22, includes a square lid that would provide improved support against tipping and sinking into the sand. The caisson wall is made from 0.024-inch thick stainless steel sheet, the caisson lid is made from 0.06-inch thick stainless steel sheet, and the center tube is made from low-carbon steel 1-1/2-inch OD tubing with 0.049-inch wall thickness. The caisson maximizes the allowable volume with a diameter of 30 cm and a height of 20 cm. The center tube is 18 cm long, such that the top of the tube will be level with the top of the testing tank when the caisson lid is flush with the sand bed. The assembly was welded together with mild steel MIG wire in

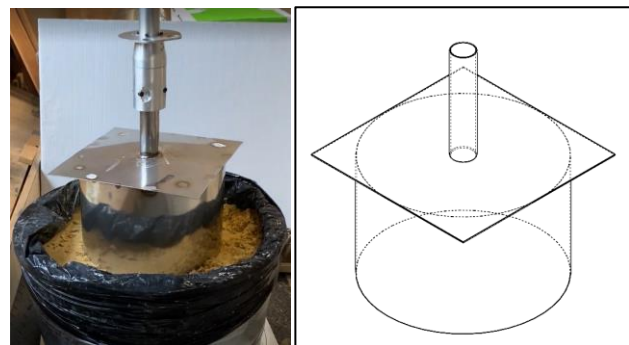


Figure 22. Caisson-type foundation prototype (left) and mechanical drawing (right)

accordance with the ferrous metal constraint. The circumference of the walls were not welded airtight to allow air to escape during installation.

To test the dynamic load response of the foundation to the operating turbine, we conducted integrated turbine tests with successful results. These results are discussed in Section 5.2.

During this testing, we saw that the caisson lid flexed, though it did not plastically deform. Though the flexing did not put the tower deflection over the 25 mm limit, we would like to minimize vibrations for more consistent power production. Prior to competition, we will add gussets around the center tube and bracing supports on the top plate to remediate this flexing.

### 2.5.2 Yaw System Design

Since no yaw turntable is incorporated in this year's competition, we decided to make a lock-able yaw system with set screws, as shown in Figure 23. The yaw housing in the nacelle interfaces with the tower top via a sleeve bearing to facilitate rotation. Given the tower diameter of 2 in (50.8 mm), M10 set screws were chosen to ensure proper contact between the set screw and the tower. Two set screws are placed 180 degrees apart. The holding power of the set screws was validated in an isolated test, shown in Figure 24, which yielded a safety factor of 5 relative to the expected yawing moment on the turbine (Appendix A). The yaw lock in the assembled turbine has also experienced wind tunnel testing up to 22 m/s with no failures.

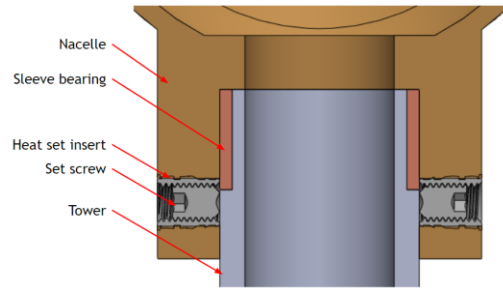


Figure 23. Section view of yaw system

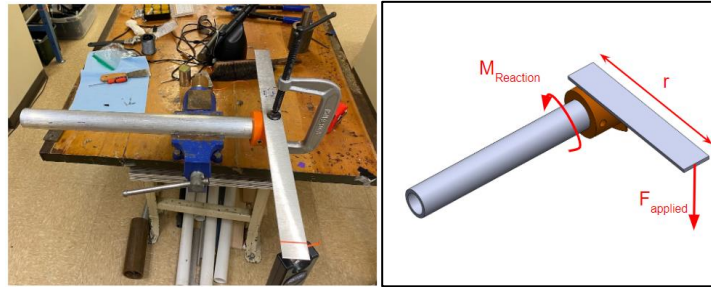


Figure 24. Isolated yaw testing

### 2.5.3 Tower-Base Assembly

The tower-base assembly is made from a 6061-aluminum plate and tube welded at the joint. The tower has an inner diameter of 1.5 in to ensure there is room for all of the electronics wires. The tower also has a hole to allow the pitot tube tubes to run up to the pressure sensor in the nacelle.

## 2.6 Enumeration of Influence of Previous Design Reports

Our performance in previous competitions have helped us identify multiple areas of improvements; however, they also provided a strong basis for this year's turbine design.

Past Designs	Influence to Current Designs
Actively pitched 3-blade rotor by linear actuator.	Same active pitch system powered by higher voltage (6 V) for increased maximum load torque.
Considered both a look-up table of optimal angles for different wind speeds and a real-time feedback	Look-up table approach based on wind speed data instead of shaft rotational speed.

---

control approach.

---

Blade modeled from S1210 airfoil (CWC21).

Main tip region of blade modeled from S1210 airfoil due to its good aerodynamic performance. Root region modeled from the thicker FX63-137 airfoil for structural support.

---

Safety stop with blade feathering and solenoid based brake (inserts pin to stop shaft rotation).

Blade feathering and caliper disc brake for safety stop, for improved power consumption and continuous friction-based braking.

---

Power relay based safety system.

Similar design with improved reliability through the use of printed circuit boards and interrupts.

---

Theoretical calculations motors for power production capabilities and chose BL23E22 model.

Improved theoretical motor comparisons and chose BL23E48.

---

## 2.7 Static Performance Analysis

### 2.7.1 $C_p$ -TSR curve

With our fully integrated turbine, we experimentally generated a  $C_p$  versus tip speed ratio plot using our on-campus wind tunnel from wind speeds 5-11 m/s (Figure 24). At each wind speed, we tested every combination of blade pitch angle and load resistance and recorded rotational speed, voltage, and current data. For this plot, we have defined our  $C_p$  as generator power output divided by the total power in the wind. In the literature,  $C_p$  is often defined as the aerodynamic captured power over the wind power, but for ease of measurement we chose to use the generated power. This is likely the reason that our plot does not look as smooth as simulated plots. Our generator operates more efficiently at the higher wind speeds and means that the same pitch and TSR can have a different  $C_p$  if the points were taken at different wind speeds. The maximum  $C_p$  occurs at a TSR of 3.7 and the blade pitch angle is defined to be 0 at the position with maximized  $C_p$  during the variable speed region.

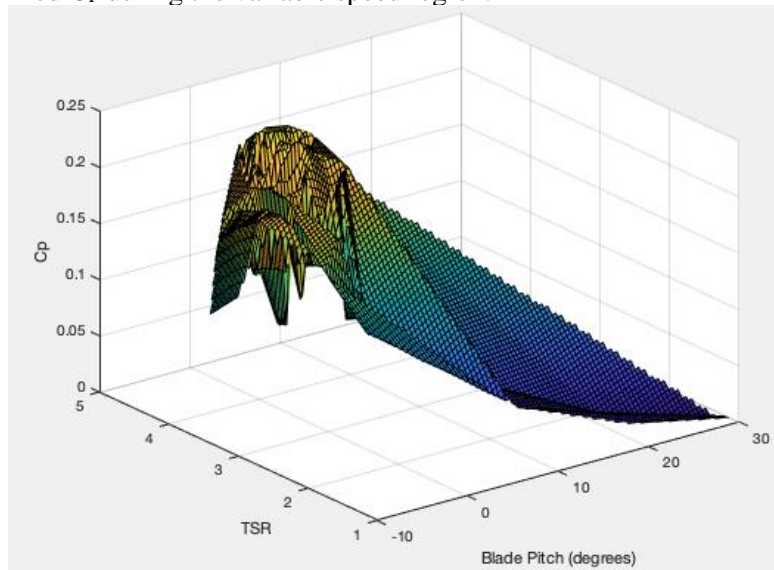


Figure 24. Experimental  $C_p$  vs. TSR plot

### 2.7.2 Annual Energy Production

The maximum possible energy output would occur if the wind speed at the location of the turbine were always at or above 11 m/s. Our turbine produces 29 W at 11 m/s, so over a year this would equal 254 kWh/yr. Using a year of hourly wind speed data from NREL for the Gulf of Mexico [13], we can assume that we will be producing no power when the wind is below 5 m/s or above 14 m/s. Using our measured power values for each wind speed including rated power from 12-14 m/s, we can calculate an annual energy production of 86.4 kWh/yr, giving a capacity factor of 35%.

## 3 Full Turbine Integration

### 3.1 Integration

The nacelle was designed to have an aerodynamic profile to maximize power captured from the wind and reduce drag force on the turbine to mitigate tipping of the foundation. We made the nacelle frontal profile as small as possible given the size of the generator and the mechanical brake. We validated that the shape of the nacelle was streamlined with a computational fluids dynamics (CFD) analysis run in COMSOL Multiphysics, shown in Figure 25. The simulation was run for steady-state, turbulent flow. We assumed laminar, uniform inflow at 22 m/s, atmospheric pressure at the outlet, no-slip wall conditions, and 20°C ambient temperature. We approximated the turbine rotor as a perforated plate. The simulation returned a drag force of 0.824 N on the nacelle, which we deemed acceptable as this value was 35 times less than the maximum expected thrust force on the rotor at 22 m/s.

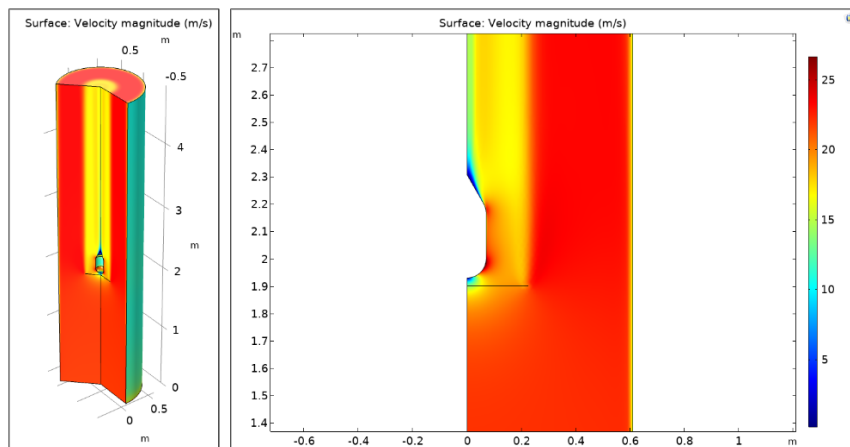


Figure 25. Velocity magnitude results of CFD analysis of nacelle in 22 m/s wind speed

We 3D-printed the nacelle in three parts. In the center nacelle section, there are two T-slot rails that run parallel through the middle of the nacelle for mounting. The two rails are spaced slightly apart to allow wires to enter the tower between them. The rails can be slid out of the nacelle to make the internal parts accessible. To fasten the front, middle, and back nacelle sections together, we used brass heat set inserts around the circumference of the surface to provide stronger threads for bolts in the plastic 3D printed part.

To support the shaft and compensate for shaft deflection at high rotational speeds, we are using self-aligning bearings. We calculated the expected radial load on the bearing to ensure our bearings were rated adequately (Appendix A). The bearings were mounted in a housing printed at 80% infill with PC blend, which has higher strength than PLA. This will help avoid fatigue failure from oscillating radial loads.

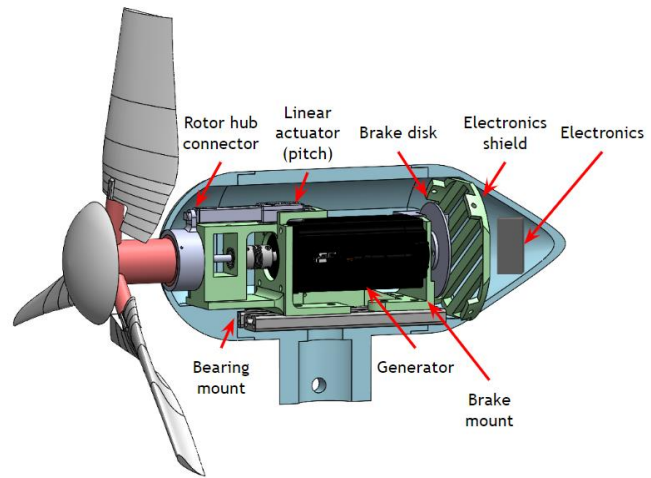


Figure 26. Section view of nacelle mechanical drawing

### 3.2 Distributed team management

For each of our engineering subteams, we initially tried to get as many students involved as possible, regardless of their background. As subteam leads, we made critical design decisions while leading manufacturing and testing. Auxiliary tasks such as conducting research for airfoil selection, searching for electronic parts compliant with competition rules, and assisting with machining were assigned to newer members with little experience in mechanical and electrical design. Students were also introduced to software such as QBlade and SolidWorks, where they learned to run aerodynamic analyses on turbine blades as well as model components for the turbine, such as the pitot tube mount. By involving these students into the project and equipping them with the skills and experience necessary to succeed, we have ensured the long-term sustainability and growth of the club for future competitions.

## 4 Commissioning Checklist

Each Commissioning Task will be performed by a team member who will initial the list after completion. Each completed task will be verified by a team member who will also initial the checklist.

Commissioning Task	Performed by	Verified by
Gather all nacelle components: nacelle (3 pieces), turbine electronics, 2 mounts, 8020 frame, 2 linear actuators, generator, mechanical brake.	DC_____	KC_____
Assemble all mechanical parts of the nacelle.	DC_____	KC_____
Place and connect all turbine electronics and peripherals in the nacelle.	ED_____	IL_____
Upload test program to turbine microcontroller and verify proper operation of both linear actuators, wind speed sensor and encoder.	ED_____	IL_____
Upload competition program to the turbine microcontroller.	ED_____	IL_____

Feed the power and signal wires (tower section) through the tower.	IL_____	ED_____
Connect the power and signal wires between the tower and the nacelle.	IL_____	ED_____
Attach electrical lead from the turbine ground to the turbine tower (which is electrically connected to the stub). Verify that the resistance between ground and tower is less than 100kOhms using a multimeter.	IL_____	ED_____
Check connectivity for the signal and power wires using a multimeter.	IL_____	ED_____
Place and secure the nacelle on the tower.	JL_____	KC_____
Secure the turbine electronics and the wires at the back of the nacelle.	JL_____	KC_____
Close and secure the nacelle.	JL_____	KC_____
Secure nose cone, blades, and rotor hub to the nacelle.	JL_____	KC_____
Gather caisson foundation and installation tools.	JL_____	KC_____
Feed the power and communication wires (foundation-PCC section) through the foundation.	JL_____	KC_____
Secure foundation into offshore simulation tank using installation tool and provided bubble level, ensuring ends of wires and all connectors stay out of water.	EL_____	KC_____
Place the tower on the foundation and connect the power and signal wires.	EL_____	KC_____
Orient the nacelle along the wind direction and secure in place.	EL_____	KC_____
Secure all load electronics are in the load enclosure and tighten the cable glands.	DC_____	ED_____
Connect the signal wires between the foundation and the load.	DC_____	ED_____
Connect power lines from turbine and load to PCC (using the Anderson Powerpole connectors).	DC_____	ED_____
Connect load to wall power.	DC_____	ED_____

## 5 Turbine Testing Results

### 5.1 Power Curve Testing

We were able to conduct testing up to 14 m/s in the Corrsin Wind Tunnel on the JHU campus. The wind tunnel is a closed loop with a 1 m tall by 1.3 m wide test section. For this test, we had to use a slightly shorter tower than would be used in competition to center the turbine rotor in the test section. With our active pitch and variable load control strategy, we were able to maximize power from 5 m/s to 11 m/s wind speeds. We were also able to produce rated power from 12 m/s to 14 m/s. Our maximum  $C_p$  was 25% at 10 m/s and our maximum power was 29 W at 11 m/s. We were able to produce rated power within 1.1% of the power produced at 11 m/s using just pitch control.

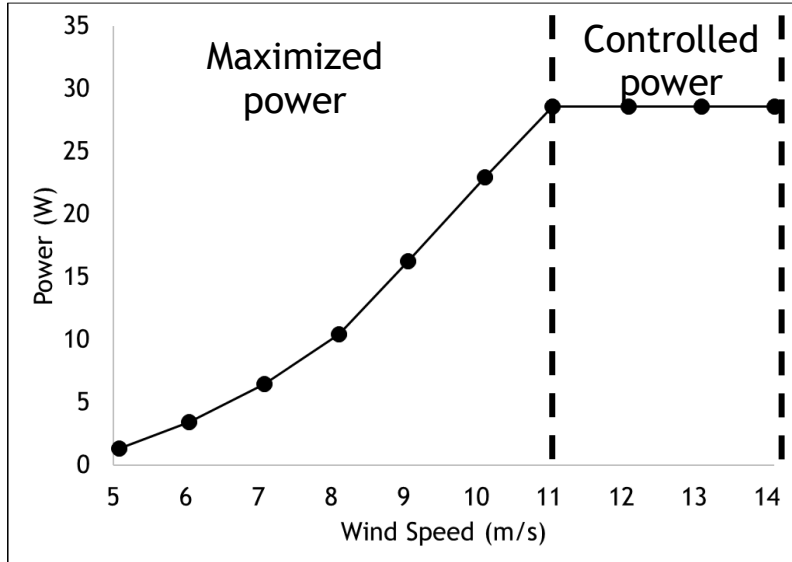


Figure 27. Power production curve

## 5.2 Durability

To test our turbine at higher wind speeds, we tested our turbine at the University of Maryland’s (UMD) Glenn L. Martin wind tunnel. Here, we mounted a tank filled with 25.4 cm of saturated sand under the test section floor to install our foundation in. We measured deflection manually with a ruler and DSLR camera using a telescoping lens (Appendix D). We conducted three tests in this wind tunnel:

1. Feathered blades without mechanical brake activated for wind speeds 15 m/s to 22 m/s with 30 seconds at each wind speed.
2. Feathered blades without mechanical brake activated at 22 m/s for 5 minutes.
3. Blades pitched for operation at 15 m/s.

The first two tests were conducted to test foundation survivability at the highest wind speeds. The third test was conducted to test foundation survivability at an operating state as close to 14 m/s as possible since we do not have the ability to test the full offshore assembly in our own campus’ facilities. The foundation passed all tests with less than 5 mm of deflection.



Figure 28. Fully-assembled turbine with offshore tank

## 6 Appendix

### 6.1 Appendix A: Expected mechanical loads and safety factors

Part	Load case	Expected load	Safety Factor
Turbine Blade (material: PC Blend)	Bending from thrust on one blade at 22 m/s*	9.4 N	7.1
Turbine Blade (material: PC Blend)	Centrifugal load at 2740 rpm	8.4 MPa	7.5

Caisson foundation	Tipping from thrust on rotor at 22 m/s**	28.2 N	1.3
Yaw housing set screws	Moment on rotor from thrust force	2.8 N·m	5.0
Pitching linear actuator [14]	Back drive thrust force on linear actuator**	28.2 N	1.6
Brake mount	Von-Mises stress from max rotor torque (Figure 15)	2.7 MPa	23.4
Braking linear actuator [14]	Braking force for maximum rotor torque***	8.73 N	1.37
Shaft bearings	Radial rotor imbalance loads****	10.1 N	247

\* The thrust on one blade is approximated as one-third of the maximum theoretical thrust on the rotor, which is 28.19N.

\*\* The theoretical thrust force at 22 m/s was calculated for the operating state, which would be a worst case scenario if the dual pitch and brake mechanisms failed; blades will be feathered and mechanical brake will be engaged past 14 m/s in competition. Thus, these safety factors are conservative.

Thrust at 22 m/s was calculated using the following equation:

$$T = \frac{1}{2} \rho A u^2 [4a(1 - a)]$$

where  $T$  is the thrust force,  $\rho$  is the density of air,  $A$  is the frontal area of the rotor,  $u$  is the wind speed, and  $a$  is the axial induction factor. The axial induction factor was conservatively chosen to be 0.33, which is the theoretical maximum. In reality, this value would be lower, decreasing the thrust on the turbine.

\*\*\* Maximum wind speed for safety stop is at 11 m/s. The maximum torque at 11 m/s is 0.155 Nm using power (28.6 W) and angular velocity (185.35 rad/s)

The required force at the point of braking is 8.73 N, using disc radius (0.0039 m) and coefficient of friction (0.455 between carbon fiber and aluminum). The braking linear actuator is capable of a 12 N backdrive force.

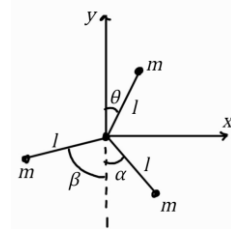
\*\*\*\* The rotor imbalance was estimated by simplifying each blade as a point mass centered on the blade's center of mass. The center of mass was evaluated on SolidWorks assuming a uniform density throughout the blade. The forces on the blades are given by the following equations:

$$R_y = m\omega^2 l(-\sin\theta + \sin\alpha - \sin\beta)$$

$$R_x = 3mg + m\omega^2 l(-\cos\theta + \cos\alpha + \cos\beta)$$

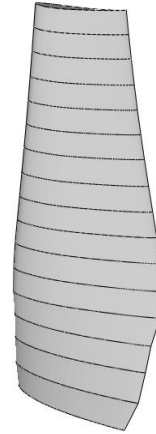
$$R = \sqrt{R_y^2 + R_x^2}$$

where  $m$  is the mass of one blade,  $\omega$  is the rotational speed of the rotor,  $l$  is the distance from the rotor center to the blade center of mass, and  $\theta$ ,  $\alpha$ , and  $\beta$  are the respective angular positions of each blade.

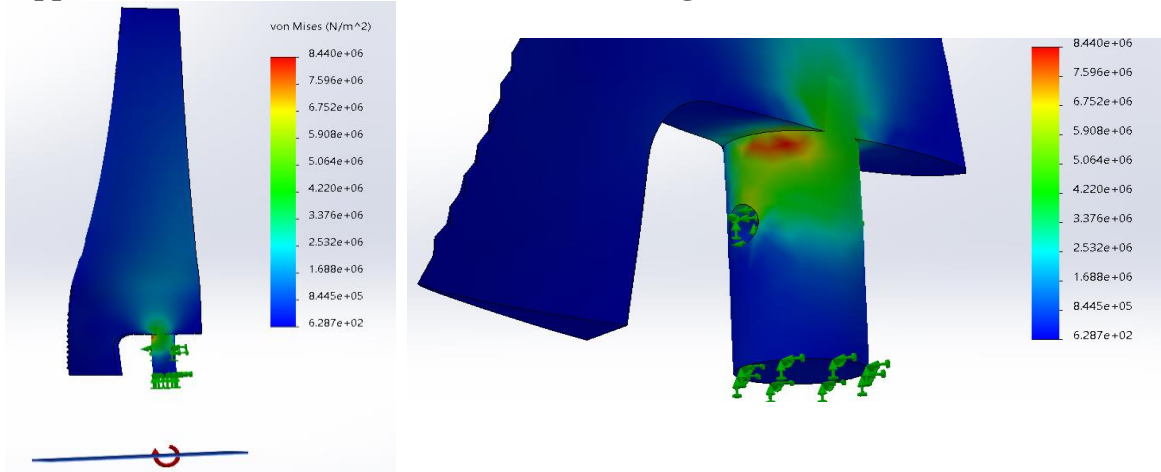


## 6.2 Appendix B: Chord/twist optimization and blade geometry from QBlade

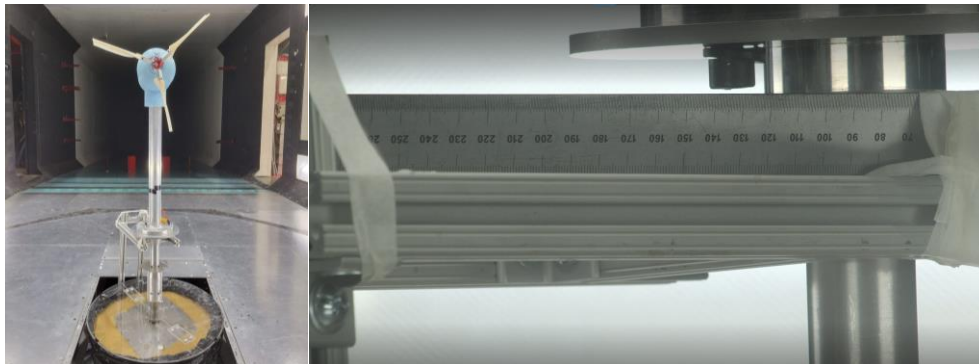
	Pos (m)	Chord (m)	Twist	Foil
1	0	0.08	39.2751	FX 63-137 13.7% smo...
2	0.011	0.08	31.586	FX 63-137 13.7% smo...
3	0.023	0.077	24.9802	FX 63-137 13.7% smo...
4	0.034	0.076	20.2	FX 63-137 13.7% smo...
5	0.045	0.076	12.3466	S1210 12%
6	0.05625	0.075	9.1362	S1210 12%
7	0.068	0.0720492	6.38479	S1210 12%
8	0.079	0.0681065	4.23872	S1210 12%
9	0.09	0.0643587	2.41797	S1210 12%
10	0.10125	0.0607774	0.82386	S1210 12%
11	0.113	0.0573245	-0.608736	S1210 12%
12	0.124	0.0543536	-1.77505	S1210 12%
13	0.135	0.0516217	-2.80221	S1210 12%
14	0.14625	0.0490563	-3.73267	S1210 12%
15	0.158	0.0466022	-4.59577	S1210 12%
16	0.169	0.0444936	-5.31863	S1210 12%
17	0.18	0.0425496	-5.97119	S1210 12%



## 6.3 Appendix C: FEA of TSR4 blades under centrifugal load (2740 RPM)



## 6.4 Appendix D: UMD Wind Tunnel Test Setup and Measured Deflection using a DSLR camera with a telescoping lens



## 7 References

- [1] Gigue`re, P., & Selig, M. S. (1998). New airfoils for small horizontal axis wind turbines. *Journal of Solar Energy Engineering*, 120(2), 108–114. <https://doi.org/10.1115/1.2888052>
- [2] Tummala, A., Velamati, R. K., Sinha, D. K., Indrāja, V., & Krishna, V. H. (2015, December 30). A review on small scale wind turbines. *Renewable and Sustainable Energy Reviews*. Retrieved October 27, 2022, from <https://doi.org/10.1016/j.rser.2015.12.027>
- [3] Salgado, V., Troya, C., Moreno, G., & Molina, J. (2016, July 23). *Airfoil Selection Methodology for Small Wind Turbines - researchgate*. Retrieved October 23, 2022, from [https://www.researchgate.net/publication/312041461\\_Airfoil\\_Selection\\_Methodology\\_for\\_Small\\_Wind\\_Turbines](https://www.researchgate.net/publication/312041461_Airfoil_Selection_Methodology_for_Small_Wind_Turbines)
- [4] *How does a wind turbine work? with GE's new ecoROTR, Better Than Ever*. GE News. (2015, June 10). Retrieved April 12, 2023, from <https://www.ge.com/news/reports/how-does-a-wind-turbine-work-with-ge-s-new>
- [5] Banggood.com. (n.d.). *JCZK 300C RC helicopter parts main rotor head set*. www.banggood.com. Retrieved April 13, 2023, from [https://usa.banggood.com/JCZK-300C-RC-Helicopter-Parts-Main-Rotor-Head-Set-p-1653921.html?cur\\_warehouse=CN&fbclid=IwAR0c-LsysOS\\_x2IZTsrhklhwDU\\_dwgOQlpMWU4o6zWOufEcoqYrnbVTMS4A](https://usa.banggood.com/JCZK-300C-RC-Helicopter-Parts-Main-Rotor-Head-Set-p-1653921.html?cur_warehouse=CN&fbclid=IwAR0c-LsysOS_x2IZTsrhklhwDU_dwgOQlpMWU4o6zWOufEcoqYrnbVTMS4A)
- [6] Prusa, J. (2022, February 16). *Technical Datasheet: Prusament PC blend by Prusa polymers*. prusament.com. Retrieved April 28, 2023, from [https://prusament.com/media/2022/10/PCBlendCF\\_Prusament\\_TDS\\_2022\\_16\\_EN.pdf](https://prusament.com/media/2022/10/PCBlendCF_Prusament_TDS_2022_16_EN.pdf)
- [7] *BL23E48-02*. Lin Engineering. (2022). Retrieved December 8, 2022, from <https://www.linengineering.com/products/brushless-motors/standard-bldc-motors/bl23-series/bl23e48-02/BL23E48-02>
- [8] DB87S01-S. Nanotec. Retrieved May 4, 2023, from <https://us.nanotec.com/products/649-db87s01-s>
- [9] DFA90S024027-A (2022). Nanotec. Retrieved May 4, 2023, from <https://us.nanotec.com/products/2886-dfa90s024027-a>
- [10] Evans, P. (2019, May 30). *Three phase voltage + calculations*. The engineering mindset. Retrieved May 4, 2023, from <https://theengineeringmindset.com/three-phase-voltage-calculations/>
- [11] Keith, J. (2023, January 31). *Capacitor input filter: Formula & calculation: ElectroSchematics*. ElectroSchematics.com. Retrieved May 4, 2023, from <https://www.electroschematics.com/capacitor-input-filter-calculation/>
- [12] Coduto, D. P., Kitch, W. A., & Yeung, M.-chu R. (2016). *Foundation design: Principles and practices* (3rd ed.). Pearson.
- [13] *Offshore gulf of mexico wind data download API: NREL: Developer network*. NREL. (2022.). Retrieved May 4, 2023, from <https://developer.nrel.gov/docs/wind/wind-toolkit/offshore-gulf-of-mexico-download/>

[14] Actuonix L12 Datasheet F. (2019) Actuonix Motion Devices Inc. Retrieved May 4, 2023, from <https://www.actuonix.com/assets/images/datasheets/ActuonixL12Datasheet.pdf>